IOWA STATE UNIVERSITY
Digital Repository

Mechanical Engineering Publications | Mechanical Engineering

2014

How do evaporating thin films evolve? Unravelling phase-separation mechanisms during solvent-based fabrication of polymer blends

Olga Wodo
State University of New York at Buffalo

Baskar Ganapathysubramanian
Iowa State University, baskarg@iastate.edu

Follow this and additional works at: http://lib.dr.iastate.edu/me_pubs


Part of the Engineering Physics Commons, Manufacturing Commons, Mechanics of Materials Commons, and the Polymer and Organic Materials Commons

The complete bibliographic information for this item can be found at http://lib.dr.iastate.edu/me_pubs/230. For information on how to cite this item, please visit http://lib.dr.iastate.edu/howtocite.html.

This Article is brought to you for free and open access by the Mechanical Engineering at Iowa State University Digital Repository. It has been accepted for inclusion in Mechanical Engineering Publications by an authorized administrator of Iowa State University Digital Repository. For more information, please contact digirep@iastate.edu.

How do evaporating thin films evolve? Unravelling phase-separation mechanisms during solvent-based fabrication of polymer blends

Olga Wodo[a] and Baskar Ganapathysubramanian[b]
Mechanical Engineering Department, Iowa State University, 2013 Black Engineering, Ames, Iowa 50011, USA

(Received 27 May 2014; accepted 3 October 2014; published online 14 October 2014)

Solvent-based fabrication is a flexible and affordable approach to manufacture polymer thin films. The properties of products made from such films can be tailored by the internal organization (morphology) of the films. However, a precise knowledge of morphology evolution leading to the final film structure remains elusive, thus limiting morphology control to a trial and error approach. In particular, understanding *when and where* phases are formed, and how they evolve would provide rational guidelines for more rigorous control. Here, we *identify four modes* of phase formation and subsequent propagation within the thinning film during solvent-based fabrication. We unravel the origin and propagation characteristics of each of these modes. Finally, we construct a mode diagram that *maps processing conditions* with individual modes. The idea introduced here enables choosing processing conditions to tailor film morphology characteristics and paves the ground for a deeper understanding of morphology control with the ultimate goal of precise, yet affordable, morphology manipulation for a large spectrum of applications. © *2014 AIP Publishing LLC*. [http://dx.doi.org/10.1063/1.4898136]

Polymer thin films have a vast spectrum of applications including drug-delivery systems, ultrahigh density storage media, and flexible electronics. In many practical applications, polymer thin films are typically fabricated using relatively simple and potentially cheap solvent-based thin-film deposition technologies.[1] Typically two immiscible polymers are dissolved in a solvent. After deposition on a substrate, solvent evaporation leads to phase separation and the final morphology. Depending on the specifics of the polymer blend and processing conditions (spin coating rate,[2] solvent type,[3] and nature of substrates[4]), different morphologies are formed in the thin film. It is essential to understand how phase separation is initiated, how it evolves to form the final morphology and how processing conditions affect morphology formation. This fundamental understanding will enable the rational design of thin films with desired structure and tailored properties.

Details of morphology evolution from initiation stage to the final morphology in solvent induced phase separation in thin films are still under debate. In this context, three mechanisms for phase-separation initiation and morphology evolution have been hypothesized: (a) phase separation induced from the modified substrate, followed by spinodal wave propagation up into the film;[5,6] (b) phase separation initiated at the top surface, followed by spinodal wave propagation down into the film;[7,8] and (c) bi-layered structure formation followed by a lateral break-up of the layers.[9,10] These hypotheses were formulated based on indirect measurements in reciprocal space such as light reflectivity,[9,10] atom force microscopy of top surface of the final structure,[5,6] or depth profile obtained from spectrometry measurements: with all measurement made in the final film only.[5] It is challenging to visualize dynamics of morphology evolution (highly dynamic processes, small length scales, and low contrast between components). Only recently Ebbens *et al.*[7] and Toolan *et al.*[11,12] directly reconstructed temporal evolution of polymer blends topography and composition via high speed stroboscopic interference microscopy. Their results support phase separation from top surface, also predicted by a few computational studies.[8] They have also showed that size of domains and type of structure can be controlled by real-time spinning rate adjustment, thus, demonstrating possibility of tailoring fabrication for desired morphology.

Building upon this exciting previous work, we pose the following questions: Are there additional mechanisms of phase-separation? Can a unifying framework clearly explain these mechanisms? To answer these questions, we use computer simulations to visualize and analyze morphology evolution for a range of blend ratios and evaporation rates. In particular, we accomplish three goals in this work: (a) using high-throughput computational analysis, we identify four mechanisms of morphology initiation and evolution; (b) we explain how these four distinct mechanisms are in fact four modes of a single instability; and (c) we show how one can map each processing condition with a unique morphology mode, thus opening up the possibility of tailoring processing conditions.

Solvent based thin film fabrication of polymer blends involves a rich and complex collection of interacting phenomena, such as fluid flow, spinodal decomposition, crystallization, substrate effects, and wetting. In this work, we focus on evaporation induced phase separation. In particular, we study the onset of spinodal decomposition along the height of thinning film. These are very few experimental studies[5–7,10–12] as it is difficult to visualize intermediate stages. On the other hand, computational approaches enable explicit tracking of the temporal and spatial distribution of individual components. Buxton and Clarke[8] reported the mode where phase separation is initiated from top surface. Several computational studies have focused on other aspects,

[a]Present address: Mechanical and Aerospace Engineering Department, SUNY at Buffalo, 125 Bell Hall, Buffalo, NY 14260, USA.
[b]Electronic mail: baskarg@iastate.edu

 © 2014 AIP Publishing LLC

such as effect of phase separation on evaporation rate and diffusion coefficient,[13] framework for exploring structure properties relationship,[14,15] or substrate effects.[4,16,17]

In this work, we use a computational framework based on phase fields to simulate morphology evolution in ternary polymer blends. In particular, we study the interplay between evaporation kinetics of the solvent from the top surface and diffusion within the film, accompanied by spinodal decomposition. A detailed description of the physical and computational models was stated by Wodo and Ganapathysubramanian.[18,19] We briefly describe the model for completeness. We consider a ternary system consisting of two components, p_1 and p_2, along with a volatile solvent, s. We denote the volume fractions of the three components as ϕ_{p_1}, ϕ_{p_2}, and ϕ_s, respectively. The total energy functional, F, assigns an energy to each possible configuration (described by ϕ_{p_1}, ϕ_{p_2}, ϕ_s) and is given by

$$F = \int_V \left[f\left(\phi_{p_1}, \phi_{p_2}, \phi_s\right) + \sum_{i=p_1,p_2} \frac{\epsilon_i^2}{2} |\nabla \phi_i|^2 \right] dV. \quad (1)$$

The interfacial energy (the second term) is scaled by an interfacial parameter,[20] ϵ. The homogenous energy (the first term), f, is given by the Flory-Huggins formulation[21,22]

$$f = \frac{RT}{V^s} \left[\sum_{i=s,p_1,p_2} \frac{\phi_i ln(\phi_i)}{N_i} + \sum_{i=s,p_1,p_2} \sum_{j \neq i} \phi_i \phi_j \chi_{ij} \right], \quad (2)$$

where R is the gas constant; T is the temperature; N_i is the degree of polymerization of component i; and χ_{ij} is the Flory-Huggins binary interaction parameter between components i and j.

The governing equations that determine the evolution of the volume fractions are derived from the free-energy functional,[14,15,17] F:

$$\begin{aligned} \frac{\partial \phi_{p_1}}{\partial t} + u \nabla \phi_{p_1} &= \nabla \cdot \sum_{j=\phi_{p_1},\phi_{p_2}} \Lambda_{\phi_{p_1} j} \nabla (\mu_j - \mu_s) + \xi_{p_1}, \\ \frac{\partial \phi_{p_2}}{\partial t} + u \nabla \phi_{p_2} &= \nabla \cdot \sum_{j=\phi_{p_1},\phi_{p_2}} \Lambda_{\phi_{p_2} j} \nabla (\mu_j - \mu_s) + \xi_{p_2}, \end{aligned} \quad (3)$$

where $\mu_i = \delta F / \delta \phi_i = (\partial f / \partial \phi_i) - (\epsilon_i^2 \nabla^2 \phi_i)$; Λ_{ij} are Onsager coefficient, ξ_{p_1} and ξ_{p_2} are the Langevin force term that mimic the fluctuation-dissipation theorem. Finally, solvent evaporation is modeled assuming that the solvent is the only component that evaporates from the top surface. The rate at which the height of the system decreases, $\frac{\partial h}{\partial t} = -k_e \bar{\phi}_s^{top}$, is proportional to the evaporation rate of the solvent out of system, k_e and the average content of the solvent at the top layer, $\bar{\phi}_s^{top}$. We assume that the solvent evaporates uniformly from the top surface and film height decreases monotonously in time. Onsager coefficients are[15] $\Lambda_{ii} = \frac{D_i}{d^2 f^{ideal}/d\phi_i^2}$, $\Lambda_{ij} = 0$.

We perform a high-throughput computational analysis with the goal to identify modes of morphology evolution and subsequently to map fabrication conditions with the modes. We specifically focus on two processing parameters: evaporation rate, k_e, and blend ratio. To ensure generality of our analysis, we non-dimensionalize the evaporation rate via Biot number.[19] The Biot number naturally accounts for the interplay between external solvent evaporation from the top layer and the internal diffusion of solvent within the film during evaporation, D_s: $Bi = k_e L / D_s$, where L is the characteristic length scale.

The system is characterized by degree of polymerization $N_{p_1} = N_{p_2} = 5$, $N_s = 1$, interaction parameters between polymers $\chi_{p_1 p_2} = 1.0$ and interaction between polymers and solvent $\chi_{p_2 s} = \chi_{p_1 s} = 0.5$. We set the interfacial energy parameter $\epsilon^2 = 10^{-10}$ J/m (typical value for organic systems[15]). The solvent self-diffusion coefficient is taken as $D_s = 10^{-9}$ m^2/s, and polymers diffusivity as $D_p = 0.2 D_s$.

Exploring a range of processing conditions ($Bi = 0.01$–10, blend ratio 1:1 to 1:0.2) resulted in the identification of four modes as depicted in Figure 1. Each mode is illustrated by 1D stacked composition profiles along the thickness at four instances. Notice that once phase-separation is initiated a sinusoidal wave is seen, indicating that some regions in the domain are p_1-rich, while others are p_1-poor. Notice also that phase separation is initiated in completely different regions for each of these four mechanisms (for full temporal evolution see movies M1–M4 in Ref. 23.)

The first mode shown, m1, corresponds to a high Biot number, $Bi = 1$, and symmetric blend ratio (1:1). Rapid evaporation of solvent from the top leads to the formation of a top boundary layer enriched in polymer. Subsequently, at $h = 0.55$, a spinodal wave forms close to the top surface and propagates downward. The wave is formed in region with the highest concentration of phase p_1 where there is a strong driving force for phase separation. This mode is in line with recent experimental observations by Ebbens *et al.*[7]

The second mode shown, m2, corresponds to a low Biot number ($Bi = 0.01$) and a symmetric blend ratio (1:1). In this case, diffusion of the solvent from the domain to the top is able to keep up with the rate at which solvent is evaporating out. The composition of the film is thus homogenous. Phase separation is initiated homogeneously along the film (see profile for $h = 0.46$), and progresses uniformly.

The third mode, m3, corresponds to $Bi = 0.2$ and blend ratio 1:0.2. Interestingly, even though we observe top boundary creation rich in at least one component, phase separation is *initiated from the bottom* (see profile for $h = 0.35$), which may appear counterintuitive. The subsequent spinodal waves propagate upward. This mode is in line with experimental observations.[5,6,24]

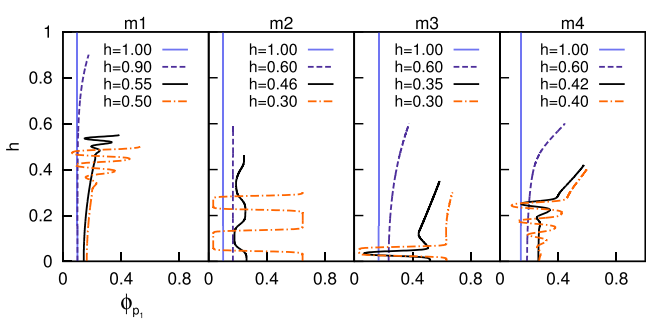

FIG. 1. The volume-fraction distribution of p_1 along normalized height at selected instances during evaporation. Each color line denotes the distribution after a certain fraction of the solvent has evaporated. The modes are denoted as m1, m2, m3, and m4.

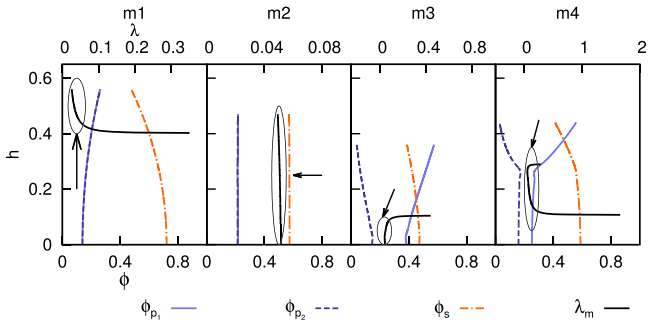

FIG. 2. Morphology evolution (1D profiles) for four modes of phase initiation (m1 to m4). Conditions just before phase initiation (1D profiles of volume fractions of three main components and the corresponding λ_m). Plot corresponds to following blend ratio and Biot number: (m1) 1:1 Bi = 1.0, (m2) 1:1 Bi = 0.01, (m3) 1:0.2 Bi = 0.2, (m4) 1:0.4 Bi = 0.5.

The forth mode, m4, corresponds to $Bi = 0.5$ and blend ratio 1:0.4. In this case, similar to the m1 and m3 modes, a top enrichment boundary forms. Phase separation, however, is initiated in the middle of the film ($h = 0.42$).

To understand and unravel the effect of processing conditions on the mechanism, we utilize linear stability analysis (LSA) (see Ref. 23 for more details). LSA allows us to characterize unstable configurations in terms of the fastest growing wavelength, λ_m. Thus, given a composition, it is possible to determine if the configuration is unstable and compute its fastest growing wavelength. The non-existence of a real, positive λ_m implies stability. Since there is a spatial distribution of composition along the film thickness, there is a spatial distribution of λ_m. The region with the lowest λ_m is the most unstable because even small fluctuations can trigger this instability. *The location of the most unstable* region in the film defines the specific mechanism of phase-separation—as shown in Figure 2—which plots each mode just before instability.

In mode 1 (first column of Figure 2), the system exhibits depletion of the solvent close to the top surface and *simultaneous enrichment of both polymers*. The system is unstable close to the top with *the lowest value of* λ_m *close to the top layer* (see λ_m distribution). Correspondingly, phase separation is initiated close to the bottom. Note that system is still stable close to the bottom, where no λ_m exists.

In mode 2 (second column of Figure 2), the composition profiles and λ_m are homogenous along the film thickness, and phase separation is initiated homogeneously along the height.

In mode 3 (third column of Figure 2), system exhibits depletion of the solvent close to top surface, as in m1. However, the top boundary shows *enrichment only in* p_1, *while exhibiting depletion in* p_2. Phase separation is initiated in the bottom and propagates upward (as seen in Figure 1). It seems counter-intuitive that phase separation is initiated at the location where content of solvent is the highest.

Using LSA argument, under conditions typical for m3, the region located close to bottom surface is characterized by the lowest value of λ_m, while zone close to the top is in stable configuration (λ_m cannot be computed for this zone and therefore is not plotted). To further confirm that the upper part of the domain is outside the spinodal region (and hence stable), in Figure 3(a) we plot the spatial distribution of compositions (black dots) on a ternary plot. We overlay the ternary plot with isocontours of λ_m to clearly identify the location of the spinodal (spinodal line is the limit of the λ_m map). A ternary plot is a elegant (and standard) way to visualize when the system enters the spinodal range (and becomes unstable). We plot three instances corresponding to three stages of morphology evolution: when the system is at the cusp of phase-separating, during initiation of phase-separation, and a short time after the initiation of phase-separation. At $h = 0.40$, the entire spatial domain is still outside spinodal range. At $h = 0.36$, only part of the spatial domain actually enters the spinodal and thus becomes unstable. We further discuss this in the supplementary material.[23] The spatial domain that has entered the spinodal region corresponds to the bottom (with the highest content of solvent, ϕ_s^{bot}). On the other hand, the upper part of the thin film has low content of solvent ($\phi_s^{top} < \phi_s^{bot}$), and corresponds to the end outside unstable zone. At $h = 0.35$, two phases form reaching equilibrium concentration: one rich in p_1 and another rich in p_2. Interestingly, even at this stage, the top part of the domain remains in the stable zone (as seen by the leg in the composition map in Figure 3 (right)).

Finally, we notice that the composition of the system exhibits a wide range of values (as seen in Figure 3(a)). This is a manifestation of the propensity of the system to dissipate its energy. This can be visually represented by plotting the composition distribution on the energy landscape. In Figure 3(b), we plot the homogenous energy landscape overlaid with the composition distribution (mode m3, $h = 0.36$). This figure shows that by following the path (marked in red) along lines of constant blend ratio the homogenous energy would need to increase. The energetically favorable pathway is the one that leads to enrichment of polymer p_1, and depletion of polymer p_2 in the top layer.

In mode 4 (last column of Figure 2), similar to mode m3, we see top boundary depletion in the solvent,

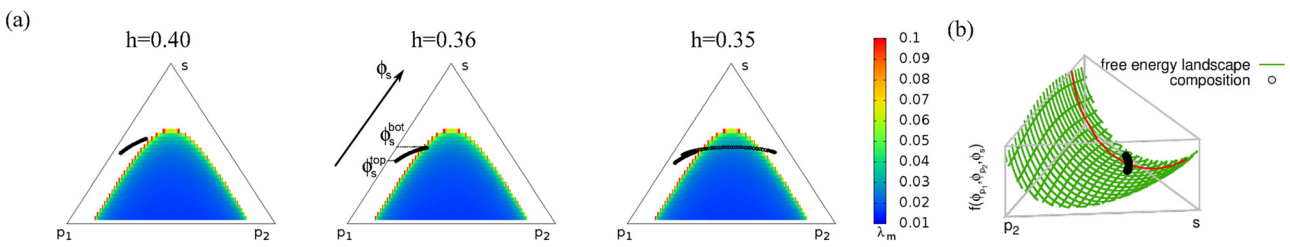

FIG. 3. (a) Morphology evolution for mode m3 of phase separation. (b) Homogenous energy landscape with distribution of composition (black dots) overlaid and iso-contour following blend ratio 1:0.2 (red curve). For temporal evolution of composition path see movie M5 in Ref. 23.

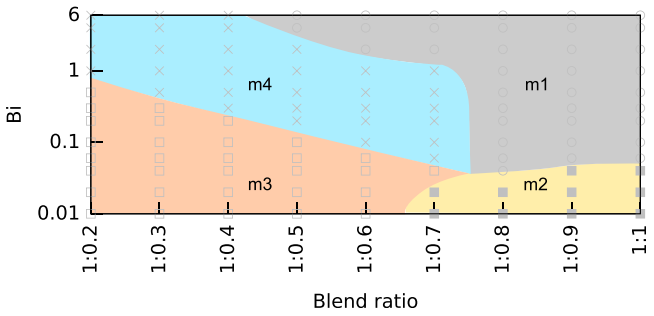

FIG. 4. Mode diagram mapping fabrication variables to four initiation modes of phase separation.

enrichment in p_1 and depletion in p_2. However, the region with distinctly lower λ_m is located in the middle of the film, where indeed phase separation is initiated. Notice that in top and bottom regions no λ_m exists, indicating stable configuration. Interestingly, in this mode, phase separation is initiated in the zone with moderate content of solvent. It appears that simply identifying regions with the lowest solvent content is not a good predictor as to where phase separation is initiated. In contrast, inspecting system instability and plotting the fastest growing wavelength provide good predictive metric of phase separation.

Finally, we map processing conditions that lead to each individual mode—see mode diagram in Figure 4. We identify two pairs of modes. Modes m1 and m2 are typical for blend ratios close to a symmetric blend ratio. Mode m2 is chosen for low evaporation rates (and Biot number) where diffusion is the dominant process. Mode m1 is expressed for high Biot numbers where evaporation is the dominant process. Modes m3 and m4, in turn, are predominant for asymmetric blend ratios. Mode m3 is typical for low Biot numbers, while mode m4 tends to be dominant for high Biot numbers. The mode diagram elucidates the link between processing and morphology formations. Its construction (enabled using high throughput computing) constitutes an important step toward process optimization. It reveals subset of processing parameters that are promising and for which additional modification may prove highly effective. For instance, substrate templating can effective prove effective to direct the morphology for mode m3.

In summary, we have identified four mechanisms of phase-separation and have shown that the location of lowest λ_m estimated from LSA tracks the location where phase-separation is initiated and thus the mechanism chosen for phase-separation. The mode chosen depends on material properties and fabrication process conditions. Specifically, it depends on the kinetics (evaporation rate and diffusion coefficients) as well as the thermodynamics (materials specific parameters defining free energy landscape) of the system. High throughput computing in conjunction with LSA can serve as a guiding link between process and system variables and morphology evolution mode, and opens up the possibility of morphology tailoring via process control.

This research was supported in part by the National Science Foundation through XSEDE resources provided by TACC under grant number TG-CTS110007. BG & OW were supported in part by NSF CAREER 1149365, and Global Collaborative Research, King Abdullah University of Science and Technology: CRG-1-2012-THO-015-ISU.

[1]F. Krebs, "Fabrication and processing of polymer solar cells: A review of printing and coating techniques," Sol. Energy Mater. Sol. Cells **93**, 394–412 (2009).
[2]C.-W. Chu, H. Yang, W.-J. Hou, J. Huang, G. Li, and Y. Yang, "Control of the nanoscale crystallinity and phase separation in polymer solar cells," Appl. Phys. Lett. **92**, 103306 (2008).
[3]K. Kawano, J. Sakai, M. Yahiro, and C. Adachi, "Effect of solvent on fabrication of active layers in organic solar cells based on poly(3-hexylthiophene) and fullerene derivatives," Sol. Energy Mater. Sol. Cells **93**, 514–518 (2009).
[4]A. Karim, J. Douglas, B. Lee, S. Glotzer, J. Rogers, R. Jackman, E. Amis, and G. Whitesides, "Phase separation of ultrathin polymer-blend films on patterned substrates," Phys. Rev. E **57**, R6273 (1998).
[5]A. Bernasik, J. Wlodarczyk-Miskiewicz, W. Luzny, K. Kowalski, J. Raczkowska, J. Rysz, and A. Budkowski, "Lamellar structures formed in spin-cast blends of insulating and conducting polymers," Synth. Met. **144**, 253–257 (2004).
[6]S. Walheim, M. Boltau, J. Mlynek, G. Krausch, and U. Steiner, "Structure formation via polymer demixing in spin-cast films," Macromolecules **30**, 4995–5003 (1997).
[7]S. Ebbens, R. Hodgkinson, A. J. Parnell, A. Dunbar, S. J. Martin, P. D. Topham, N. Clarke, and J. R. Howse, "*In situ* imaging and height reconstruction of phase separation processes in polymer blends during spin coating," ACS Nano **5**, 5124–5131 (2011).
[8]G. Buxton and N. Clarke, "Ordering polymer blend morphologies via solvent evaporation," Europhys. Lett. **78**, 56006 (2007).
[9]S. Y. Heriot and R. A. L. Jones, "An interfacial instability in a transient wetting layer leads to lateral phase separation in thin spin-cast polymer-blend films," Nat. Mater. **4**, 782–786 (2005).
[10]A. Dunbar, P. Mokarian-Tabari, A. Parnell, S. Martin, M. Skoda, and R. Jones, "A solution concentration dependent transition from self-stratification to lateral phase separation in spin-cast ps:d-pmma thin films," Eur. Phys. J. E **31**, 369–375 (2010).
[11]D. T. W. Toolan, E. Haq, A. Dunbar, S. Ebbens, N. Clarke, P. D. Topham, and J. R. Howse, "Direct observation of morphological development during the spin-coating of polystyrene–poly(methyl methacrylate) polymer blends," J. Polym. Sci., Part B **51**, 875–881 (2013).
[12]D. T. W. Toolan, A. J. Parnell, P. D. Topham, and J. R. Howse, "Directed phase separation of pfo:ps blends during spin-coating using feedback controlled *in situ* stroboscopic fluorescence microscopy," J. Mater. Chem. A **1**, 3587–3592 (2013).
[13]M. Tsige and G. S. Grest, "Solvent evaporation and interdiffusion in polymer films," J. Phys.: Condens. Matter **17**, S4119 (2005).
[14]D. M. Saylor, C.-S. Kim, D. V. Patwardhan, and J. A. Warren, "Modeling microstructure development and release kinetics in controlled drug release coatings," J. Pharm. Sci. **98**, 169–186 (2009).
[15]D. Saylor, C.-S. Kim, D. Patwardhan, and J. Warren, "Diffuse-interface theory for structure formation and release behavior in controlled drug release systems," Acta Biomater. **3**, 851–864 (2007).
[16]Y. Shang, D. Kazmer, M. Wei, J. Mead, and C. Barry, "Numerical simulation of phase separation of immiscible polymer blends on a heterogeneously functionalized substrate," J. Chem. Phys. **128**, 224909 (2008).
[17]J. J. Michels and E. Moons, "Simulation of surface-directed phase separation in a solution-processed polymer/pcbm blend," Macromolecules **46**, 8693–8701 (2013).
[18]O. Wodo and B. Ganapathysubramanian, "Computationally efficient solution to the Cahn–Hilliard equation: Adaptive implicit time schemes, mesh sensitivity analysis and the 3D isoperimetric problem," J. Comput. Phys. **230**, 6037–6060 (2011).
[19]O. Wodo and B. Ganapathysubramanian, "Modeling morphology evolution during solvent-based fabrication of organic solar cells," Comput. Mater. Sci. **55**, 113–126 (2012).
[20]J. W. Cahn and J. E. Hilliard, "Free energy of a nonuniform system. I. Interfacial energy," J. Chem. Phys. **28**, 258 (1958).
[21]L. Robeson, *Polymer Blends: A Comprehensive Review* (Hansen, 2007).
[22]G. Strobl, *The Physics of Polymers* (Springer, 2007).
[23]See supplementary material at http://dx.doi.org/10.1063/1.4898136 for additional details.
[24]A. C. Arias, N. Corcoran, M. Banach, R. H. Friend, J. D. MacKenzie, and W. T. S. Huck, "Vertically segregated polymer-blend photovoltaic thin-film structures through surface-mediated solution processing," Appl. Phys. Lett. **80**, 1695–1697 (2002).